Title no. 97-S42

Improved Analytical Model for Shear Strength of Circular Reinforced Concrete Columns in Seismic Regions

by Mervyn J. Kowalsky and M. J. Nigel Priestley

Revisions to the three component model for seismic shear strength of circular columns developed at UCSD are discussed in this paper. The revisions suggested account for the effect of the concrete compression zone on the mobilization of the transverse steel, as well as the effect of aspect ratio and longitudinal steel ratio on the strength of the concrete shear resisting mechanism.

The proposed model is compared with the previous UCSD model, as well as the design approaches of the ATC-32 and Caltrans Memo 20-4 through the use of an experimental database consisting of 47 circular reinforced concrete bridge columns. For comparative purposes, the proposed model is also compared with the ATC-40 assessment approach. Results are presented in the form of the ratio of experimentally recorded strength to design strength versus various key design parameters.

Keywords: columns; ductility; seismic; shear.

INTRODUCTION

Due to its brittle nature, shear is regarded as a mode of failure that should be avoided in reinforced concrete bridge column design. To provide a reinforced concrete bridge column with sufficient shear strength, it is imperative that the shear strength be predicted in an accurate and dependable manner.

There have been various attempts at characterization of shear strength, ranging from detailed finite element analysis to simple hand calculations such as the ACI 318,[1] ASCE/ACI 426,[2] and ATC-32.[3] The objective of this paper is to discuss the revisions of a simple assessment and design model for reinforced concrete columns that was developed at UCSD.[4] The UCSD model has two unique aspects that are generally not considered, namely, the separation of the axial load from the concrete contribution into its own shear strength mechanism, and a concrete mechanism strength that degrades with increasing ductility. Three revisions to the UCSD model are proposed in this paper to account for:

1. Effect of concrete compression zone on steel truss mechanism;
2. Effect of aspect ratio on the concrete shear resisting mechanism; and
3. Effect of longitudinal steel ratio on the concrete shear resisting mechanism.

ATC-32 SHEAR DESIGN EQUATIONS

In the following, all equations are given in S.I. units, and the shear strength reduction factor is ignored.

Nominal shear strength V_N is given by

$$V_N = V_c + V_s \tag{1}$$

where

$$V_c = 0.167\left[k_1 + \frac{P_e}{k_2 A_g}\right]\sqrt{f'_c}\,(0.8A_g) \tag{2}$$

$$V_c = \frac{\pi}{2}\frac{A_{hb} f_{yh} D'}{s} \tag{3}$$

In Eq. (2), k_1 = 1.0, except in the end regions of ductile columns, where k_1 = 0.5, and k_2 = 13.8 for compressive axial load P_e, and k_2 = 3.45 for tensile axial load where P_e has the negative sign. In Eq. (3), A_{hb} is the cross-sectional area of the hoop or spiral, with yield strength f_{yh}, and hoop spacing or spiral pitch s. The core diameter, measured to the centerline of the hoop or spiral, is D', and A_g is the column gross section area.

Assuming the defintion of ductile means a displacement ductility of $\mu_\Delta > 1.0$, then the ATC-32 equations imply a step drop in design shear strength in the column end regions when the displacement ductility reaches 1.0.

CALTRANS MEMO 20-4 ATTACHMENT B (M 20-4)

The Caltrans shear strength equations are primarily intended as an assessment tool for determining the shear strength of existing columns, rather than as a basic shear design model.

Nominal shear strength is given by Eq. (1), where

$$V_c = \nu_c A_e = F1F2\sqrt{f'_c}\,(0.8A_g) \le 0.33\sqrt{f'_c}\,A_g \tag{4}$$

and Vs is given by Eq. (3). F1 and F2 are factors modifying the shear strength dependent on displacement ductility level μ_Δ and axial load level P_e/A_g respectively, given in S.I. units by

$$F1 = 0.025 \le 0.08\rho_s f_{yh} + 0.305 - 0.083\mu_\Delta \le 0.25 \tag{5}$$

$$F2 = 0 \text{ for } P_e/A_g < 0$$

$$F2 = \left(1 + \frac{P_e}{13.8A_g}\right) \le 1.5 \text{ for } P_e/A_g \ge 0 \tag{6}$$

Thus, the correction factor for compressive axial load is the same as the ATC-32 (and ACI-3181) factor for nonductile columns (or nonductile regions of columns), but the concrete shear resisting mechanisms are taken to have no strength when the axial load on the column is tensile.

ATC-40 SHEAR ASSESSMENT EQUATIONS

Nominal shear strength is given by Eq. (1), where the concrete shear resisting mechanism strength is given in Eq. (7),

ACI Structural Journal, V97, No. 3. May-June 2000.
MS No. 98-038 received March 9, 1999, and reviewed under Institute publication policies. Pertinent discussion will be published in the March-April 2001 *ACI Structural Journal* if received by November1, 2000.

Mervyn J. Kowalsky is an assistant professor in the department of civil engineering at North Carolina State University, Raleigh, NC. He is a member of ACI Committee 213, Lightweight Aggregate and Concrete. His research interests include earthquake engineering and the seismic design and analysis of concrete structures.

M. J. Nigel Priestly is a professor of structural engineering at the University of California, San Diego, Calif.

and the steel truss mechanism strength is given in Eq. (8)

$$V_c = 0.29\left[k_1 + \frac{P_e}{13.8A_g}\right]\sqrt{f'_c}\left(0.8A_g\right) \quad (7)$$

$$V_s = \frac{A_v f_{yh} D'}{0.6s} \quad (8)$$

Note that in Eq. (7), the variable k_1 equals 1 for a displacement ductility of 2 or less, and 0 for a displacement ductility greater than 2. Also note that Eq. (8) applies as stated for circular columns as well as rectangular columns.

ORIGINAL UCSD SHEAR MODEL

The UCSD-A (assessment model) model for the shear strength of reinforced concrete members expresses the nominal shear capacity of a column V_A as the sum of three separate components as shown in Eq. (9). The variable V_s represents the shear capacity attributed to the steel truss mechanism. V_p represents the strength attributed to the axial load, and V_c represents the strength of the concrete shear resisting mechanism. The assessment model was formulated to provide an average ratio of experimental to predicted shear strength of unity. For design purposes, Eq. (9) is multiplied by 0.85 to provide an effective lower bound to the database V_D. Eq. (10) is referred to as the UCSD-D model (design model)

$$V_A = V_s + V_p + V_c \quad (9)$$

$$V_D = 0.85V_A \quad (10)$$

Note that the 0.85 is not the commonly used shear strength reduction factor of f_s= 0.85, which would normally also be applied to provide a dependable shear strength of $f_s V_D$.

The concrete component V_c is one that degrades with increasing ductility due to widening of cracks, which results in reduced aggregate interlock. The expression for the strength of the concrete shear resisting mechanism is shown in Eq. (11).[4] The g factor, which is a measure of allowable shear stress, is shown in Fig. 1(a) versus curvature ductility, and is approximated in Fig. 1(b) versus displacement ductility. Note that the g factor reduces with increasing ductility due to the reduction in aggregate interlock as cracks widen

$$V_c = 0.8A_g\gamma\sqrt{f'_c} \quad \text{(MPa)} \quad (3)$$

The axial load component V_p recognizes the shear strength enhancement provided by axial load. The magnitude of the axial load component is taken to be the horizontal component of the diagonal compression strut that carries the axial load and forms between the top and bottom of the column. For columns in double bending, the axial load enters and leaves the column through the center of the concrete compression zones at the column top and bottom. For columns in single bending, the axial load enters through the column centroid

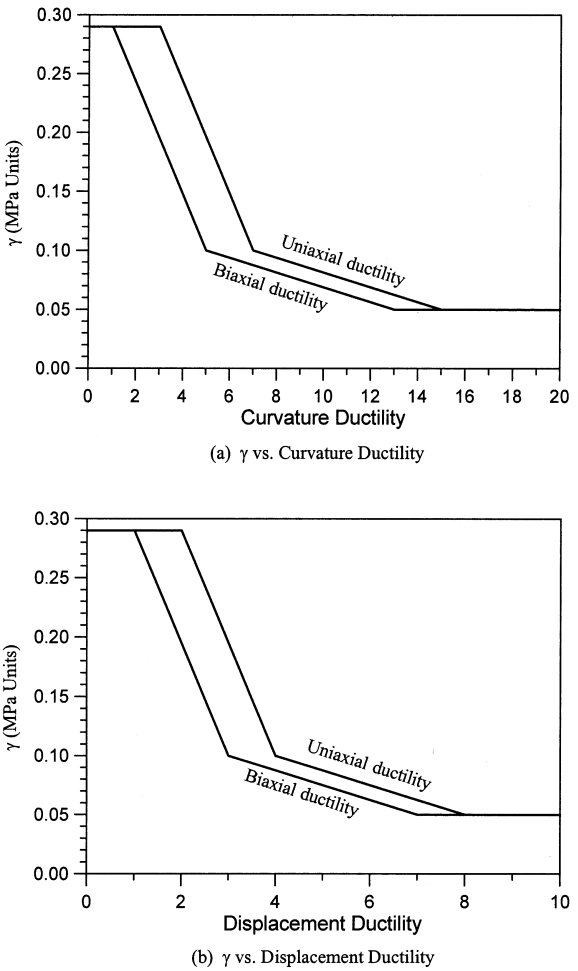

Fig. 1—γ factor—original UCSD assessement model.

and exits to the footing through the center of the concrete compression zone. The axial load mechanism is given by Eq. (12), where P is the axial load including seismic effects, D is

$$V_p = P\frac{(D-c)}{2L} \quad \text{for } P > 0 \quad (12a)$$

$$V_p = 0 \quad \text{for } P \le 0 \quad (12b)$$

the column diameter, L is the length of column from the critical section to the point of contraflexure, and c is the neutral axis depth.

The truss component strength is given by Eq. (13) for circular columns. D' is the width of the confined core diameter given by Eq. (14), where cov is the concrete cover to the outside of the longitudinal reinforcement, d_{bs} is the diameter of the transverse reinforcement, and θ represents the assumed

$$V_s = \left(\frac{\pi A_{sp}}{2} f_y \frac{D'}{s}\right)\cot(\theta) \quad (13)$$

$$D' = D - 2\,\text{cov} + d_{bs} \quad (14)$$

angle of inclination between the shear cracks and the vertical column axis. θ is assumed as 30 degrees in the UCSD-A model.

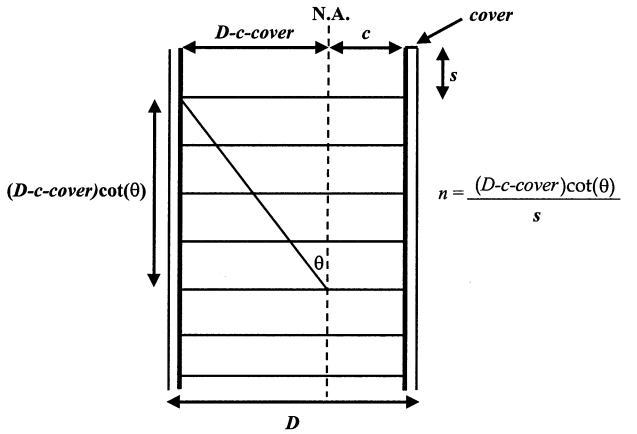

Fig. 2—Effect of concrete compression zone on truss mechanism.

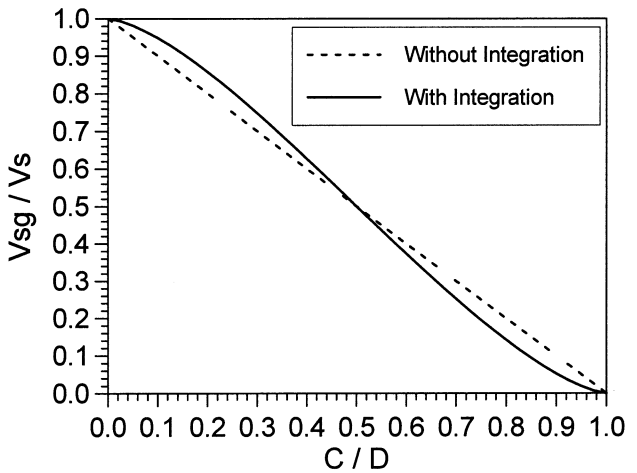

Fig. 3—Revised truss mechanism strength.

REVISED UCSD MODEL

Truss mechanism

The development of the truss analogy for shear strength of reinforced concrete members is generally credited to the engineers Ritter (1899) and Morsch (1902) as noted by MacGregor. Their work resulted in the expression shown as Eq. (15).

$$V_s = \left(A_v f_y \frac{D'}{s} \right) \tag{15}$$

Although Eq. (15) has been applied to both circular and rectangular sections, it is not exactly correct for circular sections as it implies that the effective steel area is twice that of the spiral area (although somewhat less as a reduced section depth is generally assumed). Ang et al.[6] recognized this and derived an equation for the steel truss mechanism in circular columns, which is shown as Eq. (13).[6] Refer to the work of Ang et al.[6] for a derivation of Eq. (13).

In the derivation of the truss mechanism equation of Ang et al.,[6] it was assumed that a diagonal crack is able to mobilize transverse reinforcement along a crack length extending the full width of the confined core of the concrete. In the compression zone of the column, however, any cracks are, by definition, closed. Therefore, if the crack is closed, shear cannot be transferred across it by tension strain in the transverse reinforcement. From Fig. 2, it is apparent that a reduced column width of *D*-*c*-cov is appropriate for calculating the number of spirals or hoops mobilized by the cracks between the compression struts. With reference to Fig. 2, a revised truss component equation given by Eq. (16)[7] can be obtained. Note that in Eq. (16), the effective spiral area is now a function of the neutral axis depth

$$V_{sg} = \frac{\int_{x=-(r-c)}^{r} 2A_{sp} f_y \frac{\sqrt{r^2 - x^2}}{r} dx}{D - c - \text{cov}} \frac{D - c - \text{cov}}{s} \cot(\theta) \tag{16}$$

Eq. (16) can be approximated by Eq. (17), where the integration is removed and the effective spiral area is approximated as $(\pi/2)A_{sp}$

$$V_{sga} = \frac{\pi}{2} A_{sp} f_y \frac{D - c - \text{cov}}{s} \cot(\theta) \tag{17}$$

The ratio of Eq. (17) and (16) to the traditional form given by Eq. (5) is plotted versus the c/D ratio in Fig. 3. Note that both plots show that as the neutral axis depth increases, the steel truss component strength decreases. At typical values of c/D of 0.25 to 0.35, the revised truss component is 70 to 80% of the traditional relation.

The approximate equation (Eq. (17)) is shown to be very nearly equal to the exact equation, and is 5 to 10% conservative for typical values of c/D. It is therefore suggested that the added simplification achieved by removal of the integration yields acceptable results for design situations. For the work presented herein, Eq. (17) is utilized. It is also possible to use Fig. 3 as a design aid, where the steel truss mechanism strength is calculated using the traditional equation given by Eq. (13) and then multiplied by the appropriate value obtained from Fig. 3 where the value is entered for the ratio of neutral axis depth to section diameter.

Concrete mechanism

Existing approaches for shear design have incorporated effects for the column aspect ratio and longitudinal steel ratio.[2,8] It is logical that the shear strength be greater for columns with smaller aspect ratios, as the confinement effect of the adjacent members is greater in these situations. This factor has not been accounted for in the existing UCSD model, except insofar as the axial load component V_p increases as the column length decreases.

It is also reasonable that a smaller longitudinal steel ratio will result in a decrease in the strength of the concrete shear resisting mechanism. This is due to three aspects. First, dowel action from the longitudinal reinforcement will be smaller if there are fewer numbers of small diameter bars. Second, crack distribution will be more concentrated resulting in fewer, more widely spaced cracks, which, in turn, results in a decrease in the strength of the concrete aggregate interlock mechanism. Third, the smaller compression zone resulting from the reduced longitudinal steel ratio will, in turn, reduce the compression zone shear transfer. This variable was also ignored in the original UCSD model.

On the basis of these considerations, the concrete mechanism strength was revised to give

$$V_c = \alpha\beta\gamma \sqrt{f'_c} \left(0.8 A_g \right) \tag{18}$$

In Eq. (18), the factor a accounts for the column aspect

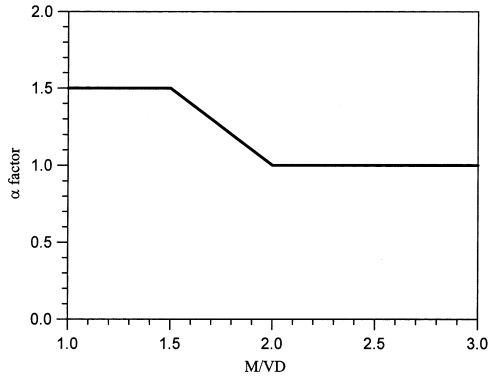

Fig. 4—α factor—revised UCSD assessment model.

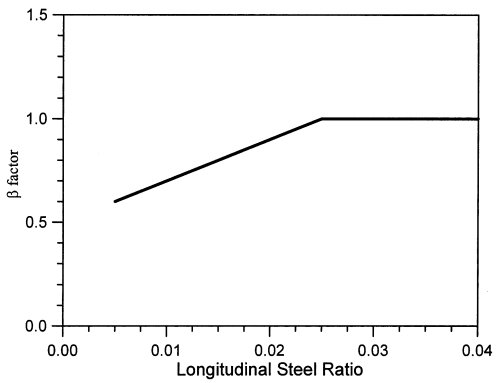

Fig. 5—β factor—revised UCSD assessment model.

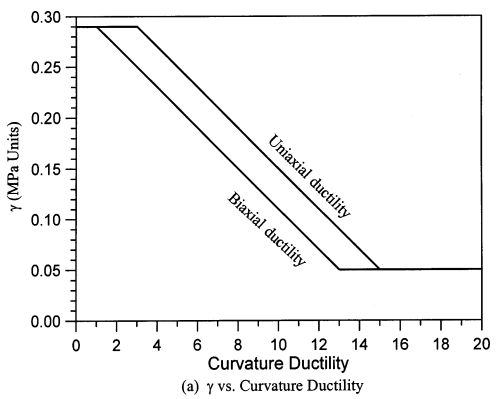

Fig. 6—γ factor—revised UCSD assessment model.

ratio, and is given by Eq. (19) (Fig. 4). The variable M/VD, where M = moment and V = shear at the critical section, is equivalent to the aspect ratio L/D, where L = distance from critical section to the point of contraflexure. Note that it is probable that the value for a continues to increase for M/VD < 1.5, but no data are currently available to confirm this.

The factor β is a modifier that accounts for the longitudinal steel ratio, and is given by Eq. (20) (Fig. 5). The axial load component given by Eq. (12) is unchanged

$$1 \le \alpha = 3 - \frac{M}{VD} \le 1.5 \tag{19}$$

$$\beta = 0.5 + 20\rho_l \le 1 \tag{20}$$

Re-examination of the test data resulted in a simplification

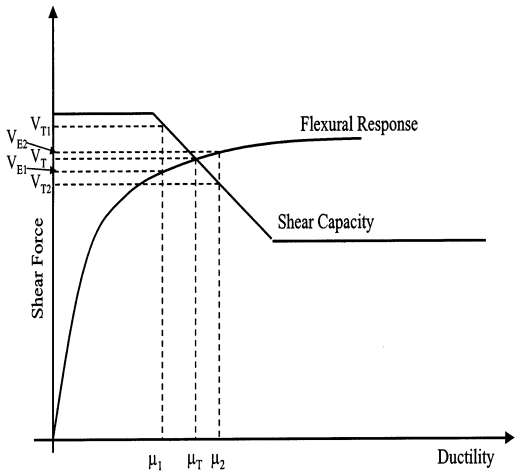

Fig. 7—Assessing shear strength using UCSD model.

of the parameter γ, which represents the reduction in strength of the concrete shear resisting mechanism with increasing ductility. The revised relationship is shown in Fig. 6.

COMPARISON OF MODELS WITH COLUMN DATABASE

To validate the proposed model, 47 columns were analyzed. Results are presented in the form of graphs relating the experimentally recorded strengths to the strengths obtained from the revised and original models. The column database is summarized in Table 1. Note that the database is divided into three categories: 1) brittle shear failures (shear failure at displacement ductility less than or equal to 2); 2) ductile failure (shear failure at displacement ductility greater than 2); and 3) ductile failures (no shear failures). Data for the latter category have been selected from circular columns with a theoretical shear strength close to the experimental maximum shear forces, but which suffered ductile flexural failure. In Table 1, the column number coincides with test number in the following graphs, and the number in square brackets is the reference for that test. Single (S) or double (D) curvature is denoted in the subsequent column, while aspect ratio is the ratio of cantilever column height to column diameter. L_{clear} represents the clear column height, f_c' is the measured concrete cylinder strength, A_h is the area of transverse reinforcement, f_{yh} is the transverse reinforcement yield stress, d_{bl} is the longitudinal bar diameter, f_y is the longitudinal bar yield stress, ρ_s is the transverse volumetric steel ratio, c is the neutral axis depth at maximum response, D is the column diameter, *cover* is the concrete cover measured to the outside of the longitudinal bars, s is the vertical spacing of transverse reinforcement, $\mu_{\Delta Exp}$ is the experimental displacement ductility at maximum recorded shear force, and P is the column axial load.

In determining the theoretical shear strength for test units with shear failures at moderate flexural ductility, some care is needed, since different interpretations are possible. With reference to Fig. 7, which shows theoretical flexural force-displacement response together with the theoretical shear strength envelope, the predicted shear strength V_T occurs at the intersection of the two curves. If the experimental ductility, however, is significantly smaller (μ_1) or larger (μ_2) than the predicted ductility (μ_T), and the theoretical flexural response is accurately predicted, then the experimental shear strengths V_{E1} and V_{E2} corresponding to m1 and μ_2 will be very close to V_T despite the large ductility discrepancy, because the flexural response is almost flat over the range of ductilities considered. A comparison based on this approach is more dependent on the accuracy of the flexural force-dis-

Table 1a Shear Column Database – brittle shear failures

Column # Source	Bend	Aspect ratio	L_{clear} (m)	f'_c (MPa)	A_h mm^2	f_{yh} (MPa)	d_{bl} (mm)	# of bars	f_{yl} (MPa)	ρ_s	c(m)	D(m)	*Cover* (m)	s(m)	P(kN)
1- [11]	S	2	1.219	26.8	18.7	200	15.9	20	454	0.0136	0.128	0.610	0.021	0.102	18.8
2- [11]	S	2	1.219	31.2	18.7	200	15.9	20	454	0.0136	0.119	0.610	0.021	0.102	18.8
3- [12]	S	2	3.048	29.6	127	298	43	24	438	0.0133	0.388	1.829	0.064	0.305	356
4- [13]	D	2	2.438	35.9	31.7	324	19	26	469	0.0254	0.172	0.610	0.020	0.127	591
5- [13]	D	1.5	1.828	31	31.7	324	19	26	469	0.0254	0.181	0.610	0.020	0.127	591
6- [14]	S	2	0.8	30.6	78.5	316	16	20	436	0.032	0.113	0.400	0.021	0.165	0
7- [14]	S	2	0.8	29.5	28.3	372	16	20	448	0.032	0.113	0.400	0.021	0.080	0
8- [14]	S	2	0.8	33.2	28.3	326	16	20	436	0.032	0.132	0.400	0.021	0.080	0
9- [14]	S	2	0.8	30.9	78.5	332	16	20	436	0.032	0.132	0.400	0.021	0.220	0
10- [14]	S	1.5	0.6	35	28.3	326	16	20	436	0.032	0.109	0.400	0.021	0.060	439
11- [14]	S	1.5	0.6	34.4	28.3	326	16	20	436	0.032	0.113	0.400	0.021	0.080	432
12- [14]	S	1.5	0.6	30.1	28.3	328	16	20	436	0.032	0.112	0.400	0.021	0.060	0
13- [14]	S	1.75	0.7	36.7	28.3	326	16	20	482	0.032	0.152	0.400	0.021	0.080	807
14- [14]	S	1.5	0.6	32.8	0.0	0	16	20	296	0.032	0	0.400	0.021	0	0
15- [15]	D	1.67	0.154	39.3	71.3	414	22.2	16	448	0.0378	0.133	0.457	0.019	0.203	0
16- [15]	D	1.67	0.154	39.3	71.3	414	22.2	16	448	0.0378	0.133	0.457	0.019	0.152	0
17- [15]	D	1.67	0.154	27.6	71.3	414	22.2	16	448	0.0378	0.149	0.457	0.019	0.203	0
18- [15]	D	1.67	0.154	27.6	71.3	414	22.2	16	448	0.0378	0.150	0.457	0.019	0.152	0
19- [16]	D	1.98	1.82	29.3	31.7	369	15.9	20	462	0.0238	0.210	0.460	0.015	0.095	1690
20- [16]	D	1.98	1.82	35.8	31.7	369	15.9	20	462	0.0238	0.095	0.460	0.015	0.095	-512

Table. 1b Shear Column Database – ductile shear failures

Column #	Bend	Aspect ratio	L_{clear} (m)	f'_c (MPa)	A_h mm^2	f_{yh} (MPa)	d_{bl} (mm)	# of bars	f_{yl} (MPa)	ρ_s	c(m)	D(m)	*Cover* (m)	s(m)	μ_Δ Exp	P(kN)
1- [13]	D	2	2.44	31	31.7	359	19	26	324	0.0254	0.166	0.610	0.020	0.127	2.79	592
2- [13]	D	2	2.44	34.5	31.7	324	19	26	324	0.0254	0.213	0.610	0.020	0.127	3.05	1780
3- [14]	S	2	0.8	37.5	28.3	328	16	20	436	0.0322	0.106	0.400	0.021	0.06	2.16	0
4- [14]	S	2	0.8	37.2	28.3	328	16	20	296	0.0322	0.089	0.400	0.021	0.06	5.68	0
5- [14]	S	2	0.8	31.1	28.3	328	16	20	436	0.0322	0.110	0.400	0.021	0.04	2.44	0
6- [14]	S	2	0.8	28.7	28.3	372	16	20	448	0.0322	0.157	0.400	0.021	0.03	4.56	721
7- [14]	S	2.5	1	29.9	28.3	372	16	20	448	0.0322	0.156	0.400	0.021	0.03	7.04	752
8- [14]	S	2	0.8	31.2	113	332	16	20	448	0.0322	0.157	0.400	0.021	0.12	4.73	784
9- [14]	S	2	0.8	29.9	28.3	372	16	20	448	0.0322	0.158	0.400	0.021	0.06	2.28	752
10- [14]	S	1.5	0.6	28.6	28.3	328	16	20	436	0.0322	0.135	0.400	0.021	0.03	3.48	358
11- [14]	S	2	0.8	36.2	28.3	326	16	20	436	0.0322	0.130	0.400	0.021	0.03	3.79	453
12- [14]	S	2	0.8	33.7	28.3	326	24	9	424	0.0326	0.108	0.400	0.021	0.06	2.64	0
13- [14]	S	2	0.8	34.8	28.3	326	16	12	436	0.0193	0.089	0.400	0.021	0.06	3.75	0
14- [14]	S	2.5	1	34.3	28.3	326	16	20	436	0.0322	0.132	0.400	0.021	0.06	2.52	429
15- [14]	S	2	0.8	32.3	113	308	16	20	436	0.0322	0.110	0.400	0.021	0.16	3.54	0
16- [14]	S	2	0.8	33.1	78.5	310	16	20	436	0.0322	0.109	0.400	0.021	0.11	3.58	0
17- [17]	D	1.5	1.83	30	28.3	361	12.7	12	462	0.0054	0.117	0.610	0.02	0.076	10.38	503
18- [17]	D	1.5	1.83	30.1	28.3	361	12.7	24	462	0.0109	0.140	0.610	0.02	0.12	3.51	503

Table 1c Shear Column Database – flexural failures

Column #	Bend	Aspect ratio	L_{clear} (m)	f'_c (MPa)	A_h mm^2	f_{yh} (MPa)	d_{bl} (mm)	# of bars	f_{yl} (MPa)	ρ_s	c(m)	D(m)	*Cover* (m)	s(m)	P(kN)	μ_Δ Exp
1- [18]	1	1.98	1.82	38.3	71	430	15.9	20	428	0.0239	0.180	0.46	0.02	0.06	1928	6
2- [18]	1	1.98	1.82	39.2	71	430	15.9	20	428	0.0239	0.082	0.46	0.02	0.06	-634	8
3- [18]	1	1.98	1.82	39.4	71	430	15.9	20	428	0.0239	0.145	0.46	0.02	0.06	970	8
4- [18]	1	1.98	1.82	35	126.7	434	15.9	30	468	0.0358	0.159	0.46	0.02	0.045	850	8
5- [18]	1	1.98	1.82	35.2	71	448	15.9	20	509	0.0239	0.103	0.46	0.02	0.08	-490	8
6- [18]	1	1.98	1.82	35	126.7	434	15.9	30	468	0.0358	0.180	0.46	0.02	0.04	1914	10
7- [19]	2	2.5	1.52	31.4	71	431	22.2	14	448	0.0185	0.160	0.61	0.025	0.097	400	6
8- [19]	2	2.5	1.52	34.6	71	431	22.2	14	448	0.0185	0.158	0.61	0.025	0.097	400	6
9- [19]	2	2.5	1.52	33.2	71	434	22.2	14	461	0.0185	0.157	0.61	0.025	0.064	400	8

placement response than on the shear strength envelope.

A more rational and more testing approach for the design equations is to use the experimentally measured ductilities directly with the shear strength envelope, without recourse to the theoretical flexural response. With respect to Fig. 7, this would result in predictions V_{T1} and V_{T2} for experimental fail-

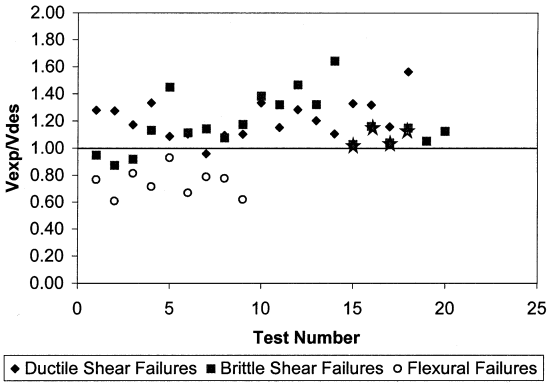

Fig. 8—Original UCSD-Design model strength ratio vs. test number.

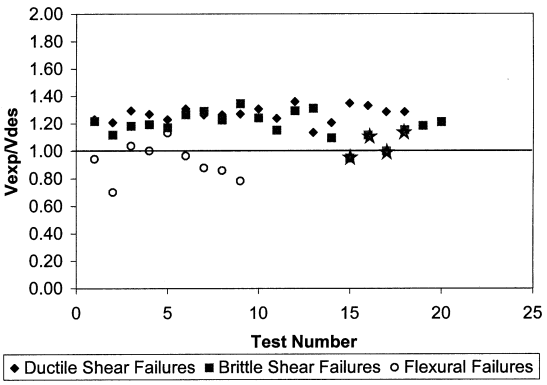

Fig. 9—Revised UCSD-Design model strength ratio vs. test number.

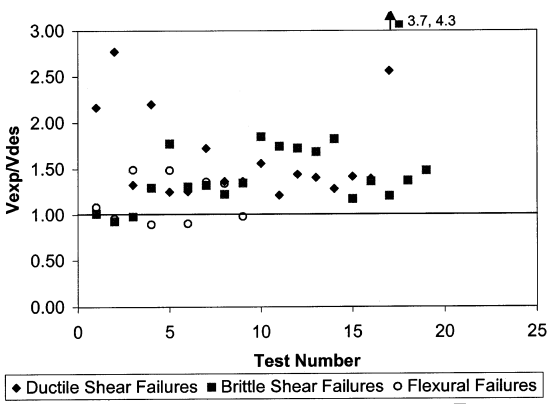

Fig. 10—Caltrans Memo 20-4 strength ratio vs. test number.

ure at μ_1 and μ_2, and much wider divergences in the V_{exp}/V_{des} ratios. This approach has been used in developing the experiment/design ratios in this paper.

In Fig. 8 to 12, the ratios of experimental shear strength to predicted shear strength are plotted against an arbitrary test number axis. This ensures that each data point is separated from the others, and facilitates direct comparison between the three design approaches. For all the figures shown, the solid diamonds represent the ductile shear failures, the solid squares represent the brittle shear failures, and hollow circles represent the flexural failures. Shown first in Fig. 8 are the ratios V_{exp}/V_{des} for the original UCSD-D model, based on Eq. (9) to (14). Note that although the scatter is not excessive, the variation for the brittle failures range from a ratio of 0.87 to 1.65. Of particular concern would be the brittle Columns 1, 2,

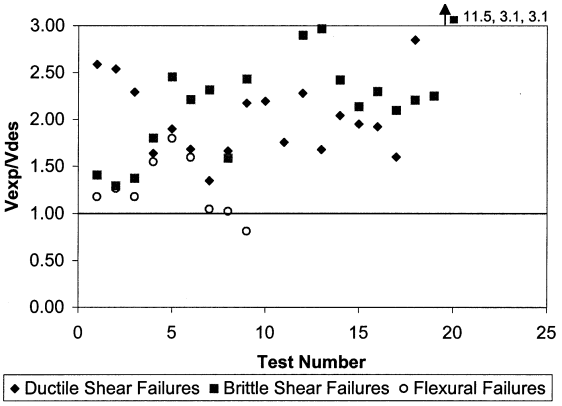

Fig. 11—ATC-32 strength ratio vs. test number.

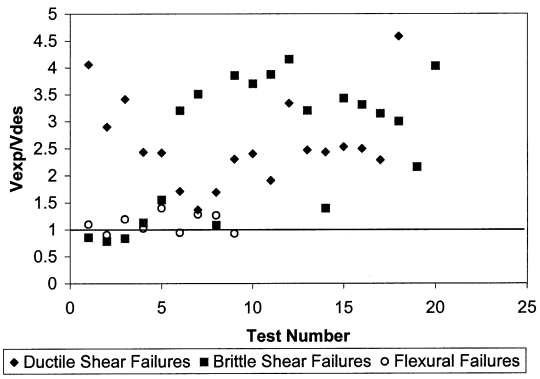

Fig. 12—ATC-40 strength ratio vs. test number.

and 3, and ductile Column 7, which all failed in shear before their predicted failure load.

The results of the revised UCSD-D model are shown in Fig. 9. From this figure, the authors note that the range of strength ratios for the brittle columns has been reduced significantly. Also, the four columns with strength ratios less than unity using the original UCSD-D model have much better results with the revised UCSD-D model. Only one data point is below the predicted strength, at 0.95. This is one of four experiments carried out by Aregawi & Collins,[13] which utilized a test unit without strong support members (foundation/cap beam) being modeled at the beam ends. These four units are represented in Fig. 8 and 9 by stars inside squares. Because of the nonstandard boundary conditions, the results should probably be omitted, but they have been included for completion. Note that all except two of the flexural failures have design strength ratios less than unity, and the close grouping of these at or near the unity line confirms the ability of the revised design equations to define the boundary between flexural and shear failures.

The results for the Caltrans Memo 20-4 model are shown in Fig. 10. Note that the vertical scale in this figure is expanded compared with Fig. 8 and 9. From this plot, the authors note significantly larger scatter than with the UCSD models, from a low of 0.9 to a high of 4.3. Two further points are worth noting from the results. First, only one of the columns failed below the expected level, indicating that the method predicts a satisfactory lower bound to strength. Second, two of the columns that suffered a flexural failure exceeded their expected shear capacity by nearly 50%. This and the rather extreme scatter indicate undesirable lack of refinement of the model.

The results for the ATC-32 model are shown in Fig. 11. From these, it is apparent that the scatter is even greater than

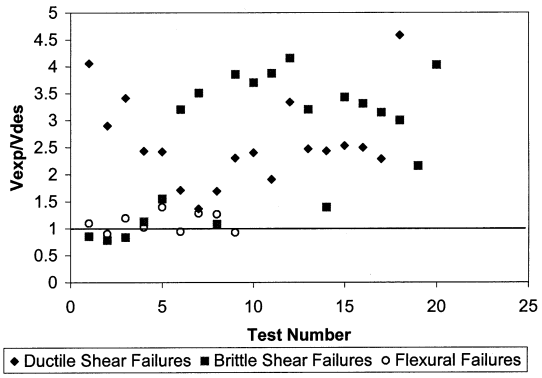

Fig. 13—Original UCSD-Assessment model strength ratio vs. test number.

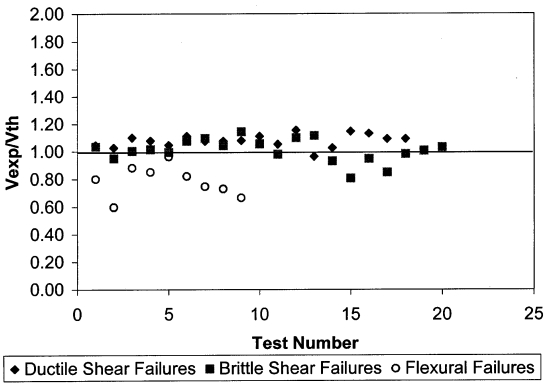

Fig. 14—Revised UCSD-Assessment model strength ratio vs. test number.

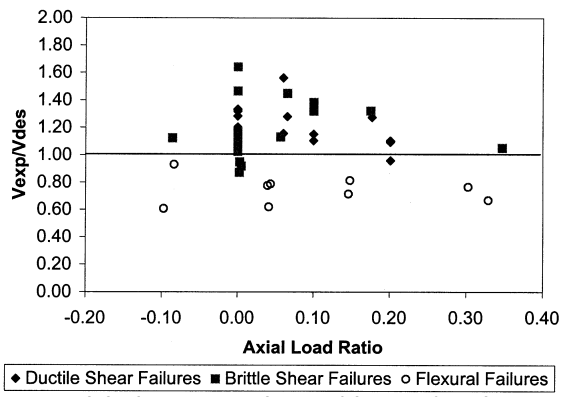

Fig. 15—Original UCSD-Design model strength ratio vs. axial load ratio.

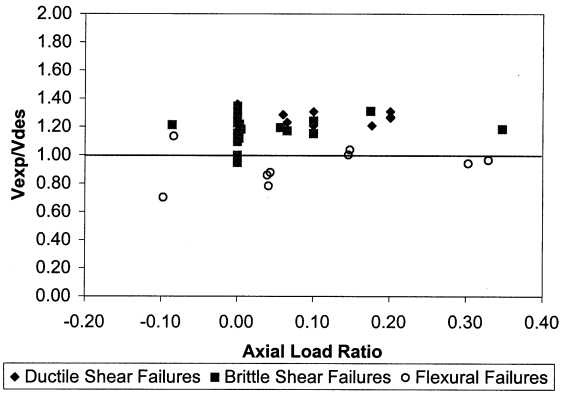

Fig. 16—Revised UCSD-Design model strength ratio vs. axial load ratio.

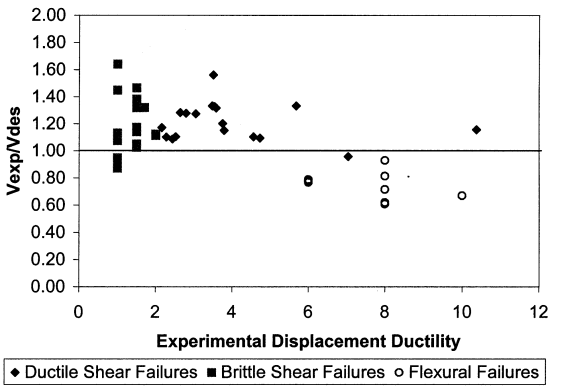

Fig. 17—Original UCSD-Design model strength ratio vs. displacement ductility

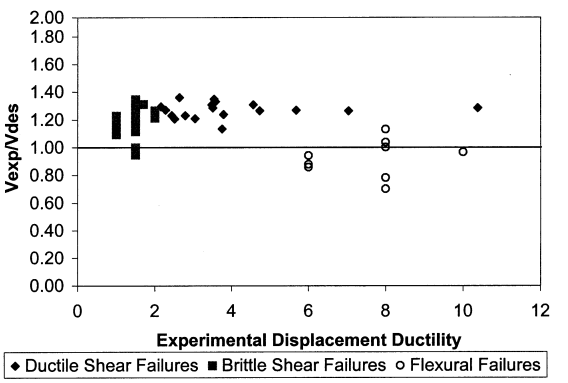

Fig. 18—Revised UCSD-Design model strength ratio vs. displacement ductility

for the Memo 20-4 approach. The range for shear failures was from a low of 1.25 to a high of 11.5 for a column subjected to axial tension. It is also noted that the ATC-32 model is intended to be a design model rather than an assessment approach, and that varying degrees of conservatism are expected. The scatter in some cases, however, is excessive.

The results for ATC-40 are shown in Fig. 12. Note that the vertical scale in Fig. 12 is plotted from 0 to 5 to capture the many data points beyond a strength ratio of 3. The scatter is excessive for this approach, particularly for the brittle shear failures that range from 0.8 to 4.2. In fairness, however, the results are usually conservative, and the extreme errors associated with the ATC-32 and Memo 20-4 approaches are absent from the ATC-40 approach. It is, however, important to note that the ATC-40 approach did not predict shear failures in brittle Columns 1, 2, and 3, which in fact did sustain a shear failure.

For completion, the results for the UCSD-A model are shown in Fig. 13 and 14. From these figures, it is noted that the revised model clearly improves the results with the exception of the Aregawi columns, which were previously discussed.

The remaining figures compare the revised and the original UCSD-D model. In Fig. 15 and 16, the data is arranged versus axial load ratio. From these plots, there appears to be a clear trend towards decreasing conservatism with increasing

Table 2 Statistical results for shear strength evaluation

	Original UCSD-D	Revised UCSD-D	Memo 20-4	ATC-32	ATC-40	Original UCSD-A	Revised UCSD-A
Brittle Shear	1.18 ± 0.20	1.19 ± 0.10	1.54 ± 0.70	2.68 ± 2.10	2.61 ± 1.23	1.00 ± 0.17	1.01 ± 0.08
Ductile Shear	1.21 ± 0.14	1.27 ± 0.06	1.74 ± 0.67	2.00 ± 0.40	2.59 ± 0.82	1.03 ± 0.12	1.08 ± 0.05

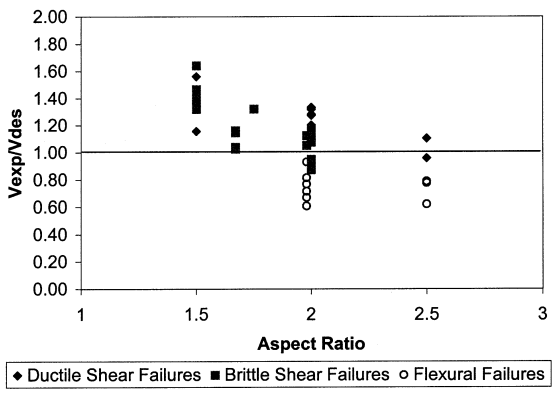

Fig. 19—Original UCSD-Design model strength ratio vs. aspect ratio.

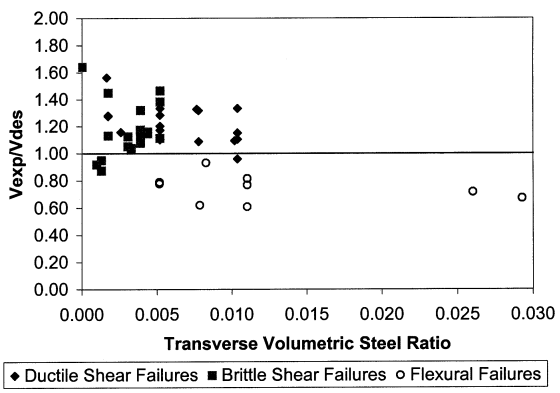

Fig. 21—Original UCSD-Design model strength ratio vs. transverse volumetric steel ratio.

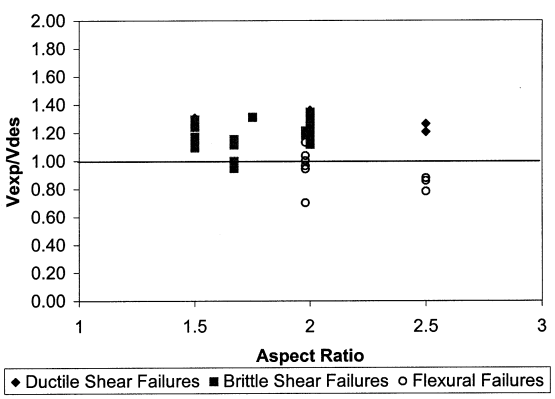

Fig. 20—Revised UCSD-Design model strength ratio vs. aspect ratio.

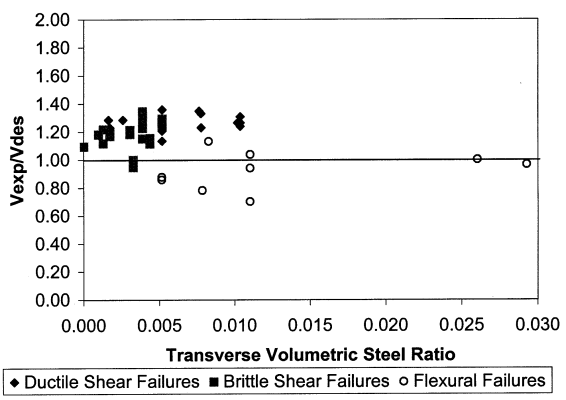

Fig. 22—Revised UCSD-Design model strength ratio vs. transverse volumetric steel ratio.

axial load in the original model, which has been corrected in the revised model. This is primarily the result of the influence of increased axial load reducing the effectiveness of the truss mechanism strength by increasing compression zone depth.

Figure 17 and 18 arrange the results according to experimental displacement ductility. In this case, the trend for the original model was a decrease in conservatism with increasing ductility, while for the revised model, no trend is apparent.

Figure 19 and 20 illustrate the results for the data arranged according to aspect ratio. Herein, the effect of the aspect ratio modification, which comes into effect below an aspect ratio of 2, is clear. For the original model, the brittle failures at a low aspect ratio were the most conservative. After the modification, which increases the strength for lower aspect ratios, the conservatism decreases proportionally.

Figure 21 and 22 arrange the data according to transverse volumetric steel ratio. Herein, the effect of the steel truss mechanism modification is clearly seen. In the original model, the strength of the columns with a significant steel contribution (high transverse steel ratio) was, in one case, nonconservative, and in the case of the assessment model, it was nonconservative for several cases. By recognizing the reduced

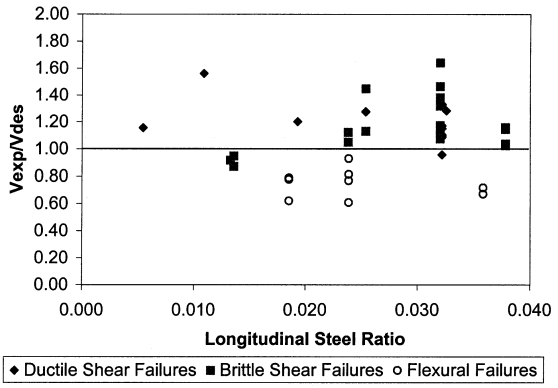

Fig. 23—Original UCSD-Design model strength ratio vs. longitudinal steel ratio.

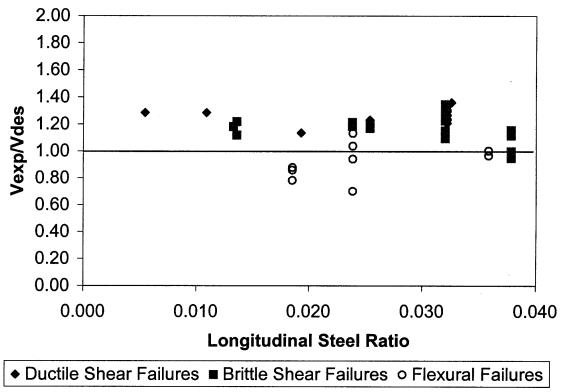

Fig. 13—Revised UCSD-Design model strength ratio vs. longitudinal steel ratio.

steel contribution, the expected strength has been lowered, resulting in more acceptable results, as shown in Fig. 22.

The last arrangement is shown in Fig. 23 and 24, where the data are arranged according to longitudinal steel ratio. Herein, the modification based on the longitudinal steel ratio is evident, as the columns with longitudinal steel ratios less than 2.5% whose strength was overpredicted using the original UCSD-D model provide more reasonable results with the revised model, as shown in Fig. 24.

A summary of the average and standard deviation for the test series is shown in Table 2 arranged according to brittle and ductile failures. From this, note that for brittle failures, although the average is essentially the same, the standard deviation for the revised UCSD-D model has improved significantly. For the Memo 20-4, ATC-32, and ATC-40 approaches, the average and standard deviation are much worse, particularly the ATC-32 approach, although that is due mainly to the column that was off by a factor of 11.5. The UCSD-A model is shown in the last columns, again indicating the improved standard deviation for the revised model.

For the ductile failures, the revised model has improved the standard deviation significantly, although the average values are slightly worse. The Memo 20-4, ATC-32, and ATC-40 approaches each have poor results, although the standard deviation is somewhat less than for the brittle failures.

CONCLUSIONS

Revisions to a three component shear strength model developed previously at UCSD were presented. The revisions include modifications for the effect of neutral axis depth, aspect ratio, displacement ductility, and longitudinal steel ratio. The revised model was compared with the original model, as well as the models of ATC-32,3 ATC-40,18 and the Caltrans Memo 20-4.19 The comparison was made through an analysis of a column database spanning 47 columns.

The revised model was shown to improve the overall scatter of the experimental database when compared with the original model. It was also shown that the UCSD shear model provides much better correlation with data than the ATC-32, ATC-40, and Caltrans approaches.

REFERENCES

1. ACI Committee 318, "Building Code Requirements for Structural Concrete (ACI 318-95) and Commentary (318R-95)," American Concrete Institute, Farmington Hills, Mich., 1995, 369 pp.

2. ASCE/ACI Joint Task Committee 426, "Shear Strength of Reinforced Concrete Members," *Journal of Structural Engineering*, ASCE, V. 99, No. ST6, June 1973.

3. Applied Technology Council, "Improved Seismic Design Criteria for California Bridges: Provisional Recommendations," *Report* No. ATC-32, Redwood City, Calif., 1996.

4. Priestley, M. J. N.; Verma, R.; and Xiao, Y., "Seismic Shear Strength of Reinforced Concrete Columns," *Journal of the Structural Division*, ASCE, V. 120, No. 8, Aug. 1994.

5. MacGregor, J. G., *Reinforced Concrete: Mechanics and Design*, Prentice Hall, 1992.

6. Ang, B. G.; Priestley, M. J. N.; and Paulay, T., "Seismic Shear Strength of Circular Reinforced Concrete Columns," *ACI Structural Journal*, V. <?>, No. <?>, Jan. 1989, pp. <?>.

7. Kowalsky, M. J.; Priestley, M. J. N.; and Seible, F., "Shear Behavior of Lightweight Concrete Columns under Seismic Conditions," *Report* SSRP-95/10, Structures Division, University of California, San Diego, Calif., 1995

8. "NZS 3101 Part 1: The Design of Concrete Structures," Standards Association of New Zealand, 1995.

9. McDaniel, C. C.; Benzoni, G.; and Priestley, M. J. N., "Scale Effects on the Shear Strength of Circular Reinforced Concrete Columns," *Report* SSRP-97/02, Structures Division, University of California, San Diego, Calif., 1997.

10. Ohtaki, T.; Benzoni, G.; and Priestley, M. J. N, "Seismic Performance of a Full-Scale Bridge Column—As Built and As Repaired," *Report* SSRP–96/07, Structures Division, University of California, San Diego, Calif., 1996.

11. Verma, R.; Priestley, M. J. N.; and Seible, F., "Assessment of Seismic Response and Steel Jacket Retrofit of Squat Circular Reinforced Concrete Bridge Columns," *Report* SSRP–93/05, Structures Division, University of California, San Diego, Calif., 1993.

12. Ang, B. G.; Priestley, M. J. N.; and Paulay, T. "Seismic Shear Strength of Circular Bridge Piers," Research *Report* 85/5, Department of Civil Engineering, University of Canterbury, New Zealand, July 1985.

13. Aregawi, M., "An Experimental Investigation of Circular Reinforced Concrete Beams in Shear," MS thesis, Department of Civil Engineering, University of Toronto, 1974.

14. Benzoni, G.; Ohtaki, T.; Priestley, M. J. N.; and Seible, F., "Seismic Performance of Circular Reinforced Concrete Columns under Varying Axial Load," *Report* SSRP–96/04, Structures Division, University of California, San Diego, Calif., 1996.

15. Priestley, M. J. N.; Seible, F.; and Benzoni, G., "Seismic Performance of Circular Columns with Low Longitudinal Steel Ratios," *Report* SSRP–94/08, Structures Division, University of California, San Diego, Calif., 1994.

16. Vu, N. H.; Priestley, M. J. N.; Seible, F., and Benzoni, G., "The Seismic Response of Well-Confined Circular Reinforced Concrete Columns with Low Aspect Ratios," *Report* SSRP–97/15, Structures Division, University of California, San Diego, Calif., 1997.

17. Sritharan, S.; Priestley, M. J. N.; and Seible, F., "Seismic Response of Column/Cap Beam Tee Connections," *Report* SSRP–96/09, Structures Division, University of California, San Diego, Calif., 1996.

18. Applied Technology Council, *Seismic Evaluation and Retrofit of Concrete Buildings: ATC-40*, 1996.

19. Caltrans Memo to Designers 20-4, Attachment B, "Earthquake Retrofit Analysis for Single Column Bents," Aug. 1996.